Optik - International Journal for Light and Electron Optics 268 (2022) 169739

Contents lists available at ScienceDirect

Optik - International Journal for Light and Electron Optics

journal homepage: www.elsevier.com/locate/ijleo

Original research article

Surface-plasmon-like distributions in metallic square shield array

D.M. Calvo-Velasco [a,*], Feng Wu [b]

[a] Departamento de Ciencias Básicas, Corporación Universitaria Comfacauca, 190001, Santander de Quilichao, Colombia
[b] School of Optoelectronic Engineering, Guangdong Polytechnic Normal University, Guangzhou 510006, China

ARTICLE INFO

Keywords:
Photonic crystals
Plasmon polariton
Revised plane wave method
Transversal electric polarization

ABSTRACT

In this work, we present the numerical study of 2D photonic crystals (PCs) made of square metallic shields distributed in a square arrangement embedded in air for the transversal electric (TE) polarization in the Γ - X direction. It is presented the modification of the photonic band structure (PBS), which shows the redistribution of bands with low dispersion at lower and higher frequencies around the surface plasmon frequency (SPF) with the decrease in the width of the shield walls. Considering the distributions of $|H_z|^2$ and $|E|^2$ in the unit cell, it is observed high intensity values in the metallic region, even for low frequencies, with a distribution like surfaces plasmons, due to the interaction of the electromagnetic modes located at the inner and the exterior surfaces of the shield. Also, it is observed that the electric field is strongly localized in the inner hole of the shield at low frequencies, which is quite different from the conventional rod geometry. These results would be utilized in electric field confinement for technological applications.

1. Introduction

Photonic crystals (PCs) are micro-structures made of periodic arrangement of materials with different optical properties which exhibit unique ability to control the propagation of light beyond natural materials [1,2]. It is known that PCs have been widely used as filters, optical junctions and waveguides among others, since they possess given frequency ranges called photonic band gaps where incident light cannot propagate in PCs [3–7]. Also, it is known that photonic band gaps depend on various parameters, such as the geometric disposition of materials in the PC, their filling fraction and external agents that act over the PC among others [8–13].

A lot of research was made considering materials with electric and magnetic responses that vary with the frequency of the incident radiation (as metals, gyromagnetic materials, polar materials), being the principal difficulty the calculation of the characteristics modes of propagation that depend strongly with the geometry disposition of the materials in the PCs [14–20]. In a previous work considering 2D PCs made of rectangular metallic rods in air [13], it was observed the presence of flat bands around the surface plasmon frequency (SPF) in the PBS for the square rod case, which are related with a strong localization of the electromagnetic radiation in the surfaces of the rods. For the rectangular rod case, it was observed the modification of the band distribution with the variation of one side of the rod, due to the modification of the resonant modes of the square rod case. Also, a high intensity of the electric field in the air region between the nearest surfaces of the rods in the crystal was observed for low frequencies.

Considering metallic slabs, it is known that the interaction of surface modes depends on the width of the slab, more precisely when the length of penetration of the radiation is of order of the width of the slab [21]. We are interesting in observed if the interaction of modes exists in a 2D PC made of square metallic shield, when the width of the shield is tiny compared with the lattice parameter. For this reason, in this work, we present the calculation of the PBS for the TE polarization of 2D PCs made of

* Corresponding author.
E-mail addresses: dannycalvo@unicomfacauca.edu.co (D.M. Calvo-Velasco), fengwu@gpnu.edu.cn (F. Wu).

https://doi.org/10.1016/j.ijleo.2022.169739
Received 17 March 2022; Received in revised form 9 June 2022; Accepted 24 July 2022
Available online 30 July 2022

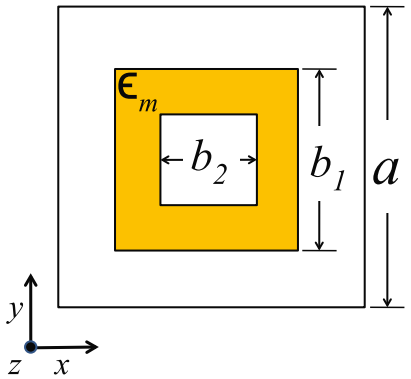

Fig. 1. Unit cell representation of a square lattice of square shields of a metallic material with dielectric function ϵ_m, surrounded by air. a is the lattice parameter, b_1 and b_2 are the lengths of the exterior and the interior sides of the square shield, respectively.

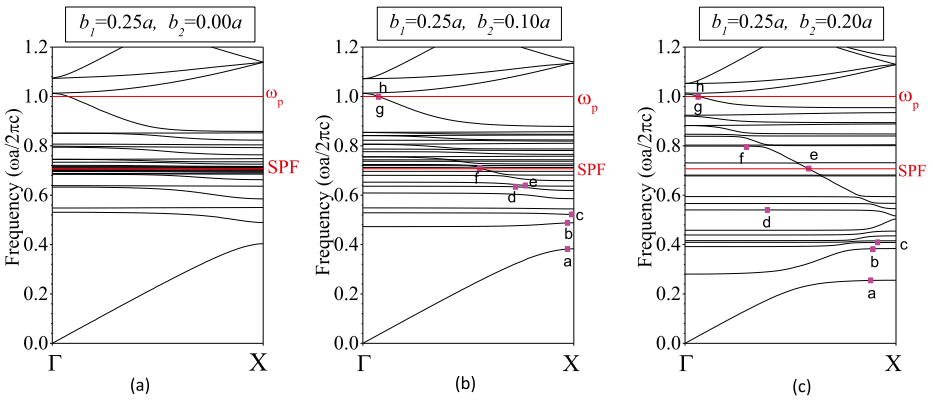

Fig. 2. Photonic band structure for TE polarization in the $\Gamma - X$ direction of a square lattice of square metallic shields in air with: (a) $b_1 = 0.25a$ and $b_2 = 0.00a$, (b) $b_1 = 0.25a$ and $b_2 = 0.10a$, and (c) $b_1 = 0.25a$ and $b_2 = 0.20a$, where a is the lattice parameter, b_1 and b_2 are the lengths of the exterior and the interior of the shield, respectively. The value of plasma frequency is $\omega_p a/2\pi c = 1.0$. Red lines show the normalized ω_p frequency and the normalized value of the SPF. The purple marked squares a - h in Figs. 2(b) and 2(c) are to display $|H_z|^2$ and $|E|^2$ as it is presented in Figs. 3 and 4 respectively.

parallel square metallic shields distribute in a square arrangement embedded in air. To understand how the PBG is modified by a square air hole in the metal, we compare the square metallic shield with the square metallic rod. Also, we calculate the distributions of $|H_z|^2$ and $|E|^2$ in the unit cell in order to understand how the field distribution is related with the PBS at some frequencies of interest.

2. Theoretical framework

The calculation of the PBS was performed using the Revised Plane Wave Method (RPWM), which considers the plane wave expansion of the electric and magnetic fields and a monochromatic response of the fields with an angular frequency ω. As it was presented in [13], for the unit cell of the PC shown in Fig. 1, the calculation of the PBS in the $\Gamma - X$ direction for the TE polarization ($\vec{H} = (0, 0, H_z)$, $\vec{E} = (E_x, E_y, 0)$) is performed when we solved the eigenvalue problem

$$k_x \begin{bmatrix} [E_y] \\ [H_z] \end{bmatrix} = \frac{1}{k_0} M \begin{bmatrix} [E_y] \\ [H_z] \end{bmatrix} \tag{1}$$

with

$$M = \begin{bmatrix} -k_0 [[G_x]] & k_0^2 - [[G_y]] [[\epsilon_{xx}]]^{-1} [[G_y]] \\ k_0^2 [[\epsilon_{yy}]] & -k_0 [[G_x]] \end{bmatrix}. \tag{2}$$

where $k_0 = \frac{\omega}{c}$, and $\left[[G_{x(y)}]\right]_{G,G'} = G_{x(y)} \delta_{G,G'}$, are diagonal matrices of order N constructed with the components of the reciprocal lattice vector $\vec{G} = (G_x, G_y, 0)$. $[E_x]$, $[E_y]$ and $[H_z]$ are column vectors of order N constructed by the coefficients of the plane wave

representation of the electric and magnetic fields. k_x is the x component of the radiation wave vector $\vec{k} = (k_x, 0, 0)$ in the $\Gamma - X$ direction.

The matrices $[[\epsilon_{xx}]]$, $[[\epsilon_{yy}]]$ are calculated following the Li's rules for the product of two periodic functions, [22,23], in our case

$$[[\epsilon_{xx}]]_{mn,m'n'} = \frac{1}{a}\int_{-a/2}^{a/2} [[A_x^{-1}]]_{m,m'}\, e^{-i(n-n')g_y y} dy, \tag{3}$$

$$[[A_x]]_{m,m'} = \frac{1}{a}\int_{-a/2}^{a/2} \frac{1}{\epsilon} e^{-i(m-m')g_x x} dx, \tag{4}$$

where $g_i = \left|\vec{b}_i\right|$ being $\vec{b}_i$ elementary translation vectors of the reciprocal lattice related with real elementary translation vectors $\vec{a}_i$ by $\vec{a}_i \cdot \vec{b}_j = 2\pi\delta_{ij}$. Also, $\epsilon(\vec{r}) = 1 + (\epsilon_m - 1)\, S(\vec{r})$, with $S(\vec{r})$ a function that is 1 in the shield and 0 in the other case. The coefficients of the matrix are relating the terms $\vec{G} = m\vec{b}_x + n\vec{b}_y$ with $\vec{G}' = m'\vec{b}_x + n'\vec{b}_y$.

A similar construction follows for $[[\epsilon_{yy}]]$.

In the presented case, the matrix $[[\epsilon_{xx}]]$ can be expanded as

$$[[\epsilon_{xx}]]_{mn,m'n'} = \begin{cases} \left[\left[A_{1,x}^{-1}\right]\right]_{m,m'} + \frac{b_1}{a}\left(\left[\left[A_{2,x}^{-1}\right]\right]_{m,m'} - \left[\left[A_{1,x}^{-1}\right]\right]_{m,m'}\right) \\ \quad + \frac{b_2}{a}\left(\left[\left[A_{3,x}^{-1}\right]\right]_{m,m'} - \left[\left[A_{2,x}^{-1}\right]\right]_{m,m'}\right) \quad , \quad n = n' \\ \frac{b_1}{a}\left(\left(\left[\left[A_{2,x}^{-1}\right]\right]_{m,m'} - \left[\left[A_{1,x}^{-1}\right]\right]_{m,m'}\right)\frac{\sin((n-n')g_y b_1/2)}{((n-n')g_y b_1/2)}\right) + \\ \frac{b_2}{a}\left(\left(\left[\left[A_{3,x}^{-1}\right]\right]_{m,m'} - \left[\left[A_{2,x}^{-1}\right]\right]_{m,m'}\right)\frac{\sin((n-n')g_y b_2/2)}{((n-n')g_y b_2/2)}\right) \quad , \quad n \neq n' \end{cases} \tag{5}$$

where

$$[[A_{1,x}]]_{m,m'} = \begin{cases} 1 \quad , \quad m = m' \\ 0 \quad , \quad m \neq m' \end{cases} \tag{6}$$

$$[[A_{2,x}]]_{m,m'} = \begin{cases} [[A_{1,x}]]_{m,m'} + \frac{b_1}{a}\left(\frac{1}{\epsilon_m} - 1\right) \quad , \quad m = m' \\ [[A_{1,x}]]_{m,m'} + \frac{b_1}{a}\left(\frac{1}{\epsilon_m} - 1\right)\frac{\sin((m-m')g_x b_1/2)}{(m-m')g_x b_1/2} \quad , \quad m \neq m' \end{cases} \tag{7}$$

$$[[A_{3,x}]]_{m,m'} = \begin{cases} [[A_{2,x}]]_{m,m'} + \frac{b_2}{a}\left(1 - \frac{1}{\epsilon_m}\right) \quad , \quad m = m' \\ [[A_{2,x}]]_{m,m'} + \frac{b_2}{a}\left(1 - \frac{1}{\epsilon_m}\right)\frac{\sin((m-m')g_x b_2/2)}{(m-m')g_x b_2/2} \quad , \quad m \neq m'. \end{cases} \tag{8}$$

A similar expression is obtained for $[[\epsilon_{yy}]]$.

Due to the non hermitian form of the eigenvalue problem presented in Eq. (1), the calculated eigenvalues are complex in general, so we chose propagating modes whose imaginary parts are near zero, i.e., $Im(k_x) \to 0$.

3. Results

According to Eq. (1), we calculated the PBS of 2D square PCs made of square metallic shields embedded in air. We considered squares shields with: (a) $b_1 = 0.25a$ and $b_2 = 0.00a$, (b) $b_1 = 0.25a$ and $b_2 = 0.10a$, (c) $b_1 = 0.25a$ and $b_2 = 0.20a$, where b_1 (b_2) is the length of the external (internal) side of the shield and a is the lattice parameter, as it was shown in Fig. 1. The dielectric function for the metal forming the shield is assumed as [24]

$$\epsilon_m = 1 - \frac{\omega_p^2}{\omega^2}, \tag{9}$$

where ω_p is the plasma frequency. In our calculations we considered $\omega_p a/2\pi c = 1.0$.

Fig. 2 presents the comparison of the PBSs calculated in the Γ - X direction for PCs made of square shields. In the case presented in (a), where a shield without interior hole (i.e., a square rod), it is observed the existence of bands with low dispersion distributed around the SPF ($\omega a/2\pi c = 0.707$), these bands are related with strong localization of the electromagnetic radiation in the rod surfaces [13]. In the case of square shields (b), it is observed a different band distribution around the SPF, in correspondence with the modification of the characteristic resonances for the rod case due to the air hole. The change in the upper frequency of the first band is observed, in correspondence with an effective lower plasma frequency value thanks to the decrease in the number of free charges in the metallic shield in comparing with the metallic rod [25]. On the other hand, it is observed the change in the slope

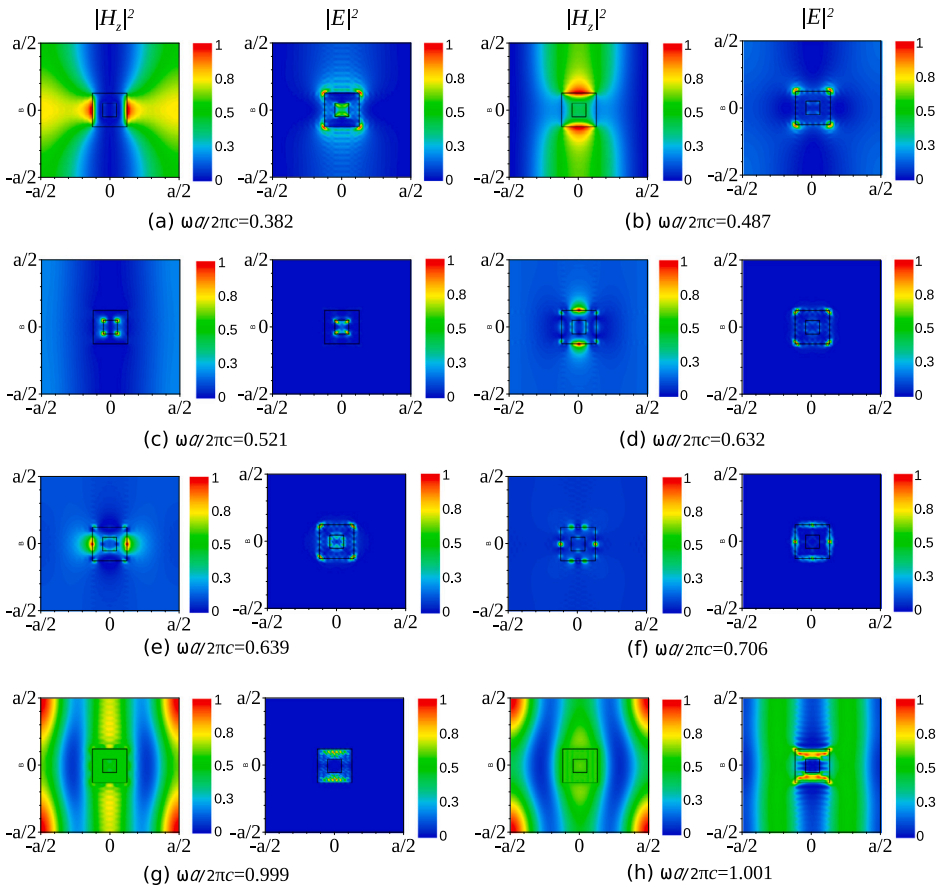

Fig. 3. $|H_z|^2$ and $|E|^2$ distributions in the unit cell of a PC made of square metallic shields with sides $b_1 = 0.25a$, $b_2 = 0.10a$ and $\omega_p a/2\pi c = 1.0$ at modes a - h in air. The intensity distribution is in arbitrary units.

for the second band and the spread of flat bands from the SPF. This must be corresponds to new optical behaviors related to the width of the metallic wall shields. In the case presented in (c) where a bigger hole is considered, the upper frequency of the first band is lower than that observed in (b) due to the continuous decrease in the effective plasma frequency of the shield. Considering the second band at the X-point its frequency has similar value of the first band in the case presented in (b). Also, it is observed the redistribution of flat bands at higher frequencies in comparing with cases presented in (a) and (b), which must be related with a strong localization of the electromanetic radiation in the shield sides. This result shows the ability of this kind of system to improve the light harvesting at higher frequencies in comparing with solid metallic rods.

Fig. 3 presents the distributions of $|H_z|^2$ and $|E|^2$ in the unit cell at the frequencies shown in Fig. 2(b). For $|H_z|^2$ in (a), it is observed a strong localization in the shield external sides, which resembles the rod case distribution at low frequencies where high negative values of the ϵ_m are reached. In contrast for $|E|^2$, high intensities are observed in the rod corners, with some in the air hole of the shield, besides, it is observed some interactions between the interior and exterior of the shield. This could be attributed to the electromagnetic penetration trough the shield walls. In this case the electric field move the electrons inside the metallic material but its move is limited by the interior or the exterior surface of the shield, where the free charges can accumulated, causing high intensity values as it was observed. This result is totally contrary to the rod case and could be used to confine electric field for technological applications. For a higher frequency as it is presented in (b), $|H_z|^2$ shows high intensity in the exterior side of the shield with some of the field located in the interior hole, as it is expected the distribution is orthogonal to the case presented in (a). For $|E|^2$, high intensity is observed in the exterior corners of the shield, with the decrease in the intensity in the shield interior region compared with (a). Also, some interaction between high intensity distributions are observed, looking as a surface mode located principally in the exterior sides of the shield parallel to the incident radiation. In this case the system geometry contributed to the formation of surface modes at lower frequencies in comparing with the square rod geometry. In the case presented in (c), $|H_z|^2$ and $|E|^2$ presented high intensities in the air hole in the shield, which is in accordance with the low dispersion for this band. It is interesting to observe that the field distribution is prohibitive in the rod case [13] and constitute and special property of the shield geometry. In the cases presented in (d) and (e) where an anticrossing is observed, $|H_z|^2$ is distributed principally in the exterior sides of the shields, for (d) in the sides parallel to the wave vector and for (e) perpendicular to the wave vector. Also, it is observed some

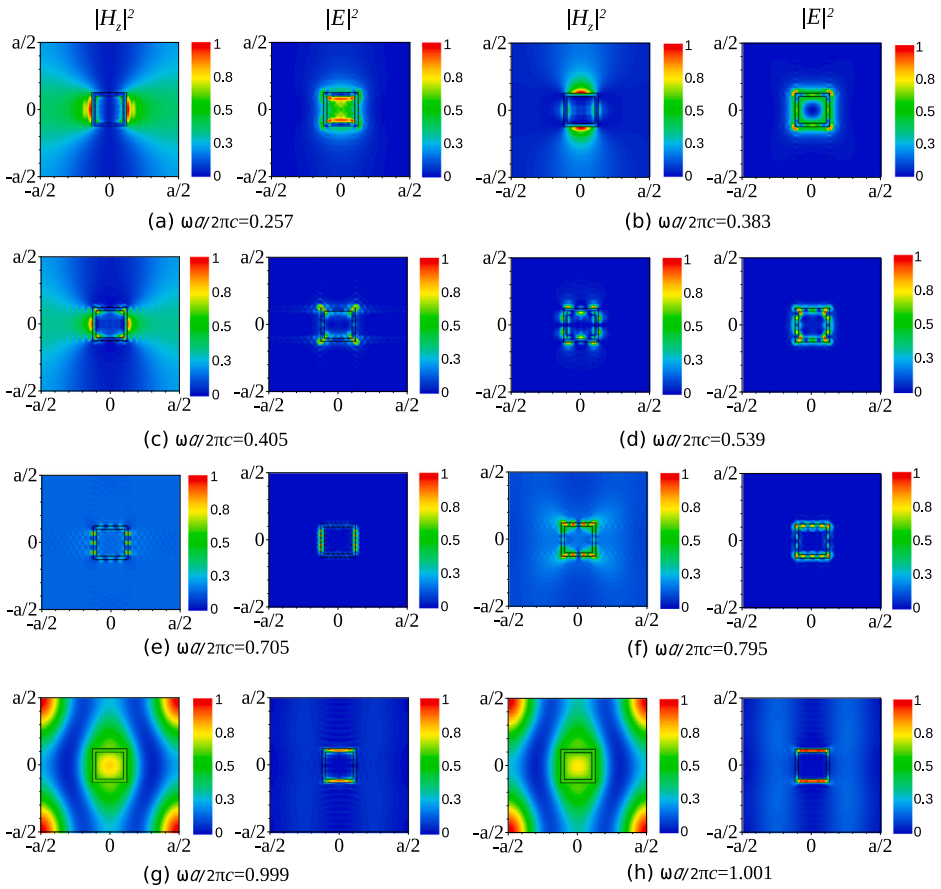

Fig. 4. $|H_z|^2$ and $|E|^2$ distributions in the unit cell of a PC made of square metallic shields with sides $b_1 = 0.25a$, $b_2 = 0.20a$ and $\omega_p a/2\pi c = 1.0$ at modes a - h in air. The intensity distribution is in arbitrary units.

interaction between the fields located outside and inside the shield, specially in the case presented in (e). Is remarkable the decrease of the field intensity in the region of the exterior surfaces occupied by the magnetic field, in comparing with (b) and (d), where high intensity values are reached. In the case of $|E|^2$ high intensities are observed principally in the exterior corners of the shield, but the exterior and the interior surfaces shows the formation of localized surface modes. This is in correspondence with band with low dispersion, but the shield geometry induces more surface where localized the radiation. Also, it is observed high interaction between the exterior and interior modes of the shield, due to the decrease in the $|\epsilon_m|$, which contributed with the increase in the penetration depth of the electric field. In the case presented in (f), for a frequency below but close to the SPF, $|H_z|^2$ shows strong localization with a decrease in the occupied surface in comparing with previous frequencies. Also, the formation of some dots with medium intensities are observed. On the other hand, $|E|^2$ is distributed in the exterior sides of the shield. In this case, the formation of a surface mode is evident. Also, the interior region of the shield has not electric radiation inside. For the cases presented in (g) and (h) where frequencies below and above but close to $\omega_p a/2\pi c$, the $|H_z|^2$ shows a distribution that is similar to the rod case [13]. In contrast in (g), $|E|^2$ is distributed mainly inside the metallic region, even when $\epsilon_m < 0$. On the other hand, for (h) the field is also distributed outside the shield with the highest intensities in the metallic material. This behavior could be used as a switch for the electric field, due to the special field distribution that change radically below and above the plasma frequency inside the material, for a tight bandwidth. Also the interior air region acts like a free electric space, and constituted as a invisibility cloak for the electric information.

Fig. 4 presents the distributions of $|H_z|^2$ and $|E|^2$ in the unit cell at the frequencies shown in Fig. 2(c). In (a), $|H_z|^2$ is mainly distributed outside the shield with high intensity in the exterior air region. In contrast $|E|^2$ is mainly distributed in the inner air region. It is noticeable that the reduce of the width of the shield walls induces a stronger localization in the inner air region at lower frequencies in comparing with the case presented in Fig. 3. Increasing the frequency to the case presented in (b), it is observed that $|H_z|^2$ is strongly localized at the exterior sides of the shield parallel to the x axis, while $|E|^2$ is distributed inside and outside the shield with a highest intensity in the exterior corners of the shield. In comparing for the distribution presented in Fig. 3(a), $|E|^2$ distributions are similar, but here a spot of low intensity is observed in the inner air region with the reduce of the width of the metallic shield. Also, the electric field is almost distributed in the metallic material even when ϵ_m is extremely negative. In (c), they

are presented the distributions at a frequency value inside the gap at the X point of systems presented in Figs. 2(a) and 2(b). $|H_z|^2$ distribution shows the formation of places with high intensity close to the shield corners in the metallic region. Also, high intensity distributions outside the shield are observed, in particular the interaction between the interior and the exterior surfaces of the shield. For $|E|^2$, it is observed a strong localization close to the shield corners in the interior air region, join to the interaction between modes that are located at the exterior and inner metallic surfaces of the shield. It is remarkable that the inner surface of the shield allows a distribution of the field like a surface mode. In (d), it is observed a strong localization of $|H_z|^2$ and $|E|^2$ in correspondence with a low band dispersion. For $|H_z|^2$, it is observed places with high intensity outside all the shield. Also, the intensity distribution shows interaction between the interior and exterior surfaces with medium intensities in the metallic material, as it was also observed in (c). For $|E|^2$, a similar distribution discussed previously in (c) is observed, where exist places with high intensity close to the corners of the shield in the metallic region as well as a strong localization in the shield sides which are extended for one metallic surface to the other. In (e), it is presented the distribution for a frequency close to the SPF. In this case, $|H_z|^2$ is strongly localized in the exterior surfaces of the shield with a propagating behavior in the PC, this is in correspondence with the non-zero value of the group velocity for this band. $|E|^2$ shows high localization in the exterior surfaces of the shield, perpendicular to the propagation direction, like surfaces plasmons which are extended from the exterior to the inner surface. In comparing with the case presented in Fig. 3(f), the field distribution is more extended and could be used in technological applications. In (f), it is observed a similar behavior as that presented in (e), but in this situation high intensity values are observed inside the metallic region. This behavior is in correspondence with the rod case at frequencies above the SPF [13], the radiation starting to enter inside the metallic region due to the low absolute value of the ϵ_m. In (g), it is presented a frequency below but close to ω_p, in this case $|E|^2$ is mainly localized inside the metal which is in correspondence with the result presented in (f) due to the low absolute value of ϵ_m. Also, the field distribution is similar to the case presented in Fig. 3(g), high intensities are reached in the metallic material. Also some similar distribution is observed in (h) for a frequency above but close to ω_p, it is observed that $|E|^2$ is mainly localized inside the metal with a low intensity outside the shield. Contrary to the case presented in Fig. 3(h), where high values of intensities are reached outside the metallic shield. In these cases the shield width is an important factor in the electric field localization. For $|H_z|^2$ it is not observed difference below and above ω_p, these distributions are as the square metallic rods case, with higher intensities in the inner air region of the shield.

At it was presented, the decrease in the width of the metallic shield modifies the field distribution, which induced high intensities values in the exterior surface of the shield appearing like localized plasmons for the electric field, in particular at frequencies close to the SPF.

4. Conclusions

As summary in this work, it was presented the numerical calculation of the PBS and the distributions of $|H_z|^2$ and $|E|^2$ in the unit cell for a PC made of square metallic shields in air. It was found the modification of the PBS with the decrease in the width of the shield walls, showing the redistribution of bands with low dispersion at higher and lower frequencies around the metallic SPF in comparing with the rod case. These flat bands are related with a strong localization of the radiation inside the metallic material, with a plasmon-like distribution also observed at low frequencies. It was found that the shield geometry favored the electric field localization inside the inner hole of the shield at low frequencies, which is quite different from the conventional rod geometry. These results would be utilized in electric field confinement for technological applications.

Declaration of competing interest

The authors declare that they have no known competing financial interests or personal relationships that could have appeared to influence the work reported in this paper.

Data availability

No data was used for the research described in the article.

References

[1] J.D. Joannopoulos, S.G. Johnson, J.N. Winn, R.D. Meade, Photonic Crystals: Molding the Flow of Light, Pricenton University Press, Pricenton, 2008.
[2] K. Sakoda, Optical Properties of Photonic Cristals, second ed., Springer-Verlag, Berlin, Heidelberg, 2005.
[3] N. Engheta, R.W. Ziolkoshowski, Metamaterials: Physics and Engineering Explorations, IEEE Press, Wiley-Interscience, 2006.
[4] Y. Fink, J.N. Winn, S. Fan, C. Chen, J. Michel, J.D. Joannopoulos, E.L. Thomas, A dielectric omnidirecional reflector, Science 282 (1998) 1679.
[5] F. Wu, K. Lyu, S. Hu, M. Yao, S. Xiao, Ultra-large omnidirectional photonic band gaps in one-dimensional ternary photonic crystals composed of plasma, dielectric and hyperbolic metamaterial, Opt. Mater. 111 (2021) 110680.
[6] G. Lu, X. Zhou, Y. Zhao, K. Zhang, H. Zhou, J. Li, C. Diao, F. Liu, A. Wu, G. Du, Omnidirectional photonic bandgap in one-dimensional photonic crystals containing hyperbolic metamaterials, Opt. Express 29 (20) (2021) 31915–31923.
[7] F. Wu, M. Chen, S. Xiao, Wide-angle polarization selectivity based on anomalous defect mode in photonic crystal containing hyperbolic metamaterials, Opt. Lett. 47 (9) (2022) 2153–2156.
[8] S.B. Cavalcanti, M. de Dios-Leyva, E. Reyes-Gómez, L.E. Oliveira, Band structure and band-gap control in photonic superlattices, Phys. Rev. B 74 (2006) 153102.
[9] J.R. Mejía-Salazar, N. Porras-Montenegro, E. Reyes-Gómez, S.B. Cavalcanti, L.E. Oliveira, Plasmon polaritons in 1D cantor-like fractal photonic superlattices containing a left-handed material, Europhys. Lett. 95 (2) (2011) 24004.

[10] L.E. González, N. Porras-Montenegro, Pressure, temperature and plasma frequency effects on the band structure of a 1D semiconductor photonic crystal, Physica E 44 (4) (2012) 773–777.
[11] J. López, L.E. González, M.F. Quiñonez, M.E. Gómez, N. Porras-Montenegro, G. Zambrano, Magnetic field role on the structure and optical response of photonic crystals based on ferrofluids containing Co0.25Zn0.75Fe2O4 nanoparticles, J. Appl. Phys. 115 (19) (2014) 193502.
[12] B. Diaz-Valencia, J. Calero, Photonic band gaps of a two-dimensional square lattice composed by superconducting hollow rods, Physica C 505 (2014) 74–79.
[13] D.M. Calvo-Velasco, N. Porras-Montenegro, High plasmon concentration on the surfaces of rectangular metallic rods embedded in air in a 2D photonic crystal, Appl. Phys. A 122 (2016) 431.
[14] V. Kuzmiak, A.A. Maradudin, F. Pincemin, Photonic band structures of two-dimensional systems containing metallic components, Phys. Rev. B 50 (1994) 16835–16844.
[15] V. Kuzmiak, A.A. Maradudin, A.R. McGurn, Photonic band structures of two-dimensional systems fabricated from rods of a cubic polar crystal, Phys. Rev. B 55 (1997) 4298–4311.
[16] V. Kuzmiak, A.A. Maradudin, Distribution of electromagnetic field and group velocities in two-dimensional periodic systems with dissipative metallic components, Phys. Rev. B 58 (1998) 7230–7251.
[17] K. Sakoda, N. Kawai, T. Ito, A. Chutinan, S. Noda, T. Mitsuyu, K. Hirao, Photonic bands of metallic systems. I. Principle of calculation and accuracy, Phys. Rev. B 64 (2001) 045116.
[18] K. Sakoda, Electromagnetic eigenmodes of a three-dimensional photonic fractal, Phys. Rev. B 72 (2005) 184201.
[19] E. Moreno, D. Erni, C. Hafner, Band structure computations of metallic photonic crystals with the multiple multipole method, Phys. Rev. B 65 (2002) 155120.
[20] Q.-B. Li, Z. Li, R.-x. Wu, Bending self-collimated one-way light by using gyromagnetic photonic crystals, Appl. Phys. Lett. 107 (24) (2015) 241907.
[21] S. Maier, Plasmonics: Fundamentals and Applications, Springer Science+Business Media LLC, 2007.
[22] L. Li, Use of Fourier series in the analysis of discontinuous periodic structures, J. Opt. Soc. Amer. A 13 (9) (1996) 1870–1876.
[23] P. Lalanne, Effective properties and band structures of lamellar subwavelength crystals: Plane-wave method revisited, Phys. Rev. B 58 (1998) 9801–9807.
[24] C. Kitell, Introduction to Solid States Physics, seventh ed., Wiley, New York, 1966.
[25] C.D. Giovampaola, N. Engheta, Digital metamaterials, Nature Mater. 13 (2014) 1115.